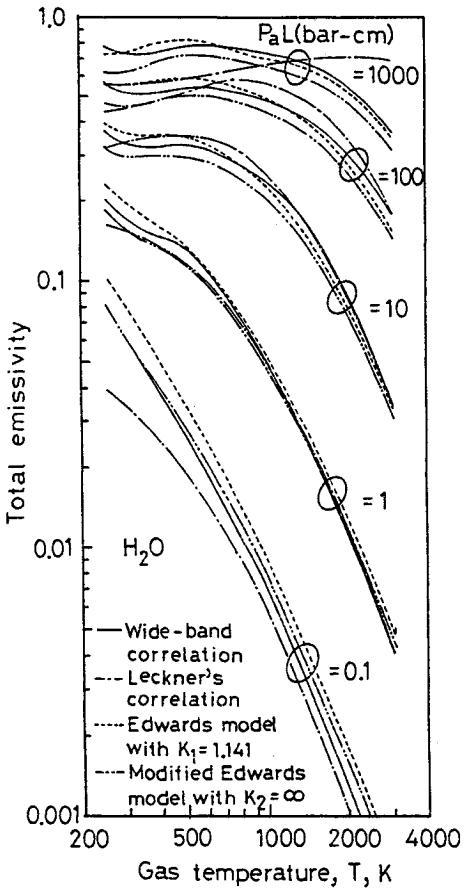


**Fig. 2 Total emissivity of water vapor at a total pressure of 10 bar and a partial pressure of 10 bar.**

et al.,[4] i.e., $K_1 = 1.0$, whereas the obtained values of $K_2$ are appreciably greater than 2.

Figure 1 illustrates the total emissivities of water vapor at a total pressure of 1 bar and 0 partial pressure. It is found from this figure that the modified Edwards model is better than the Edwards model, and thus, the modified Edwards model with the optimally adjusted free parameter can be utilized accurately at comparatively low total and partial pressures. However, as seen from Table 1, when an absorbing gas pressure is raised, the reverse is the case even for a total pressure of 1 bar.

Figure 2 depicts the total emissivities at a total pressure of 10 bar and a partial pressure of 10 bar. This figure shows that the predictions by the Edwards model are more accurate than those by the modified Edwards model. As readily understood from Table 1, this is generally true for high total gas pressures.

Finally, it is found that Leckner's correlation[6] becomes less accurate as the partial pressure-path length is increased over about 100 bar-cm.

## Conclusions

Free parameters introduced into the two wideband spectral models, i.e., Edwards model and modified Edwards model, for water vapor at various total and partial gas pressures are adjusted so as to obtain better agreement between the total emissivity computed directly from its definition and that evaluated using the exponential wideband model. It is found that the optimum values of the free parameters are different from their originally given values and that, when the free parameters optimally determined for given total and partial pressures are utilized, the Edwards model yields more accurate results in comparison with the modified Edwards model, except for low total and partial pressures. The proposed wideband spectral models for the absorption coefficient are expected to be utilized in solving various radiative transfer problems in nonisothermal and nonhomogeneous media bounded by nonblack walls.

## Acknowledgments

The authors wish to acknowledge their sincere gratitude to T. F. Smith and an anonymous reviewer for their valuable comments.

## References

[1]Edwards, D. K., and Menard, W. A., "Comparison of Models for Correlation of Total Band Absorption," *Applied Optics*, Vol. 3, No. 5, 1964, pp. 621–625.

[2]Edwards, D. K., *Advances in Heat Transfer*, Vol. 12, Academic Press, New York, 1976, pp. 115–193.

[3]Desoto, S., and Edwards, D. K., "Radiative Emission and Absorption in Nonisothermal Nongray Gases in Tubes," *Proceedings of the 1965 Heat Transfer and Fluid Mechanics Institute*, Stanford Univ. Press, Stanford, CA, 1965, pp. 358–372.

[4]Edwards, D. K., Glassen, L. K., Hauser, W. C., and Tuchscher, J. S., "Radiation Heat Transfer in Nonisothermal Nongray Gases," *Journal of Heat Transfer*, Vol. 89, 1967, pp. 219–229.

[5]Taniguti, H., Kudo, K., Otaka, M., Sumarsono, M., and Obata, M., "Development of a Monte Carlo Method for Numerical Analysis on Radiative Energy Transfer Through Non-Grey-Gas Layer," *International Journal for Numerical Methods in Engineering*, Vol. 35, 1992, pp. 883–891.

[6]Leckner, B., "Spectral and Total Emissivity of Water Vapor and Carbon Dioxide," *Combustion and Flame*, Vol. 19, 1972, pp. 33–48.

# Finite Element Analysis of the Heat Transfer in Concentric-Tube Heat Exchangers

C. L. Ko*
*Oakland University, Rochester, Michigan 48309*

## Introduction

ALTHOUGH the finite element method has been extensively used for solving structural problems as well as some heat transfer and fluid flow problems, it had never been applied to a heat-exchanger system until Mikhailov and Ozisik[1] reported their analysis using this method. Nevertheless, instead of solving energy equations for fluid flows, they assumed the overall heat transfer coefficient was given, and was a constant such that they could obtain the relationship between element heat transfer rates and nodal temperatures. Hence, their basic principle was the same as those of the classical log-mean-temperature-difference (LMTD) and the number of transfer units (NTU) methods, which only solve the thermodynamic part of the problem. Furthermore, these classical methods assume that the heat transfer is only in the radial direction for the purpose of evaluating the overall heat transfer coefficient; however, the heat transfer is also inconsistently assumed to be in the radial direction only in these methods when it comes to estimate the actual temperature variation. In the light of these shortcomings, the objective of this Note is to apply fundamental principles in physics to heat exchangers by solving the problem of momentum and energy coupling in fluids, as well as the problem of heat conduction in solid bodies simultaneously. Both the parallel-flow configuration

Received Sept. 9, 1993; revision received March 23, 1994; accepted for publication March 30, 1994. 

*Associate Professor, Department of Mechanical Engineering. Member AIAA.

and the counterflow configuration are analyzed by using the Galerkin formulation of the finite element method.

## Analysis

The heat-transport behavior of a concentric-tube heat exchanger is modeled as a steady-state axis-symmetric conjugate heat-transfer problem. Flows in the exchanger are assumed to be fully developed incompressible laminar flows, such that the exact solutions of Navier-Stokes equations for the flow in a tube (Hagen-Poiseuille flow) and the flow in a concentric annulus, as compiled by White,[2] can be utilized to obtain velocity profiles. Hence, governing equations of a concentric-tube heat exchanger can be expressed as

$$y\frac{\partial^2\theta}{\partial y^2} + \frac{\partial\theta}{\partial y} + C_1 y\frac{\partial^2\theta}{\partial x^2} - C_2 y\left(1 - \frac{y^2}{y_1^2}\right)\frac{\partial\theta}{\partial x} + 4C_3\frac{y^3}{y_1^4} = 0 \quad \text{for} \quad 0 \le y \le y_1 \tag{1}$$

$$y\frac{\partial^2\theta}{\partial y^2} + \frac{\partial\theta}{\partial y} + C_6 y\frac{\partial^2\theta}{\partial x^2} = 0 \quad \text{for} \quad y_1 \le y \le y_2 \quad \text{and} \quad 1 \le y \le y_4 \tag{2}$$

$$y\frac{\partial^2\theta}{\partial y^2} + \frac{\partial\theta}{\partial y} + C_1 y\frac{\partial^2\theta}{\partial x^2} + C_4 y\left[(y^2 - 1) + (1 - y_2^2)\frac{\ln y}{\ln y_2}\right]\frac{\partial\theta}{\partial x} + C_5\left[4y^3 + \frac{(y_2^2 - 1)^2}{y(\ln y_2)^2} - \frac{4y(y_2^2 - 1)}{\ln y_2}\right] = 0 \quad \text{for} \quad y_2 \le y \le 1 \tag{3}$$

where

$$\theta \equiv (T - T_1)/(T_3 - T_1), \quad x \equiv z/L$$

$$y \equiv r/R_3, \quad y_1 \equiv R_1/R_3, \quad y_2 \equiv R_2/R_3$$

$$y_4 \equiv R_4/R_3, \quad C_1 \equiv C_6 \equiv (R_3/L)^2, \quad C_2 \equiv \sqrt{C_1}(Pr_1 Re_1/y_1)$$

$$C_3 \equiv Pr_1 Re_1^2\{\mu_1^2/[\rho_1^2 R_1^2 c_{p1}(T_3 - T_1)]\}, \quad C_4 \equiv \pm Pr_3 Re_3^* \sqrt{C_1}$$

$$C_5 \equiv Pr_3 Re_3^{*2}\{\mu_3^2/[\rho_3^2 c_{p3}(T_3 - T_1)R_3^2]\}, \quad U_1 \equiv 2Q_1/(\pi R_1^2)$$

$$Pr_1 \equiv \mu_1 c_{p1}/k_1, \quad Pr_3 \equiv \mu_3 c_{p3}/k_3$$

$$Re_1 \equiv R_1\rho_1 U_1/\mu_1, \quad Re_3^* \equiv (\rho_3 R_3 U_3)/\mu_3$$

$$U_3 \equiv \frac{2Q_3}{\pi R_3^2[1 - y_2^4 + (1 - y_2^2)^2/\ln y_2]}$$

$$Re_3 \equiv Re_3^*(1 - y_2)\left[1 + y_2^2 + \frac{(1 - y_2^2)}{\ln y_2}\right]$$

Here, $T_1$ and $T_3$ are the maximum or minimum absolute inlet temperatures of the tube flow and the shell flow, respectively. Temperature at any location $(r, \phi, z)$ in the cylindrical coordinate system is denoted as $T$, and the length of the heat exchanger is specified as $L$. The $z$ axis is the centerline of the tube and the origin is located at the center of the tube inlet section. The inside and the outside radii of the tube are denoted as $R_1$ and $R_2$, respectively, and those radii of the shell are designated as $R_3$ and $R_4$, respectively. Densities, specific heats, thermal conductivities, and viscosities of the tube fluid and the shell fluid are designated as $\rho_1$, $\rho_3$, $c_{p1}$, $c_{p3}$, $k_1$, $k_3$, $\mu_1$, and $\mu_3$, respectively. Volume flow rates of the tube flow and the shell flow are also specified as $Q_1$ and $Q_3$, respectively. For a counterflow heat exchanger, the $z$ axis is in the opposite direction of the shell flow and, hence, the value of $C_4$ should be negative; whereas, the direction of the shell flow of a parallel-flow exchanger is the same as that of the $z$ axis, therefore, the value of $C_4$ should be positive.

It is assumed that the outer wall of the shell is insulated, and the temperature profiles of both the tube flow and the shell flow are specified at inlets. Hence, boundary conditions can be specified as

At $y = 0$ and $y = y_4$:

$$\frac{\partial\theta}{\partial y} = 0 \tag{4}$$

At $x = 0$ and $x = 1$:

$$\frac{\partial\theta}{\partial x} = 0 \quad \text{for} \quad y_1 \le y \le y_2 \quad \text{and} \quad 1 \le y \le y_4 \tag{5}$$

At $x = 0$:

$$\theta = \theta_1(y) \quad \text{for} \quad 0 \le y \le y_1 \tag{6}$$

At the inlet of the shell flow ($x = 0$ for parallel flow or $x = 1$ for counterflow):

$$\theta = \theta_3(y) \quad \text{for} \quad y_2 \le y \le 1 \tag{7}$$

Here, $\theta_1$ and $\theta_3$ are the specified inlet temperature profiles of the tube flow and the shell flow, respectively. The following heat balance and compatibility conditions at the interface between fluid flows and wall surfaces should also be satisfied:

At $y = y_1$:

$$k_1\left.\frac{\partial\theta}{\partial y}\right|_{y_1^-} = k_2\left.\frac{\partial\theta}{\partial y}\right|_{y_1^+} \quad \text{and} \quad \theta|_{y_1^-} = \theta|_{y_1^+} \tag{8}$$

At $y = y_2$:

$$k_2\left.\frac{\partial\theta}{\partial y}\right|_{y_2^-} = k_3\left.\frac{\partial\theta}{\partial y}\right|_{y_2^+} \quad \text{and} \quad \theta|_{y_2^-} = \theta|_{y_2^+} \tag{9}$$

At $y = 1$:

$$k_3\left.\frac{\partial\theta}{\partial y}\right|_{1^-} = k_4\left.\frac{\partial\theta}{\partial y}\right|_{1^+} \quad \text{and} \quad \theta|_{1^-} = \theta|_{1^+} \tag{10}$$

Respectively, $k_2$ and $k_4$ are the thermal conductivities for the tube wall and the shell wall. The flow domain at $y = y_1$ is indicated by $y_1^-$ and the wall surface at $y = y_1$ is represented by $y_1^+$. Similar distinctions at $y = y_2$ and $y = 1$ are denoted by $y_2^+$, $y_2^-$, $1^-$, and $1^+$, respectively.

The computational domain of the governing equations, $0 \le x \le 1$ and $0 \le y \le y_4$, are divided into four types of rectangular elements: 1) tube-flow elements, 2) tube-body elements, 3) shell-flow elements, and 4) shell-body elements. The Galerkin method, which employs shape functions as weighting functions, is adopted in this analysis.

The total rates of heat-energy absorption received by the tube flow, $\dot{Q}_t$, and by the shell flow, $\dot{Q}_s$, can be approximately estimated as

$$\dot{Q}_t = \dot{m}_t c_{p1}(\bar{T}_{to} - \bar{T}_{ti}) \quad \text{and} \quad \dot{Q}_s = \dot{m}_s c_{p3}(\bar{T}_{so} - \bar{T}_{si}) \tag{11}$$

where $\dot{m}_t$ and $\dot{m}_s$ are the mass flow rates of the tube flow and of the shell flow, respectively. The average inlet and outlet temperatures of the tube fluid and the shell flow are denoted as $\bar{T}_{ti}$, $\bar{T}_{to}$, $\bar{T}_{si}$, and $\bar{T}_{so}$, respectively. Because numerical results

obtained by using the finite element technique are only approximate solutions of the governing equations, and because the two expressions in Eq. (11) are also approximations, absolute values of $\dot{Q}_t$ and $\dot{Q}_s$ could be different from each other. Consequently, values of the heat-exchanger effectiveness $\varepsilon_t$ and $\varepsilon_s$, calculated by using theses two different heat transfer rates, could also be unequal.

## Experimental and Theoretical Results

Numerical results calculated by using the present analysis are compared to experimental measurements and those obtained by using the LMTD method. The experimental apparatus is a concentric-tube heat exchanger with an inner tube and an outer tube as shown in Fig. 1. Both the inner and the outer tubes were made of copper, and a 15.9-mm-thick sponge rubber was placed around the outer tube for insulation. The i.d. and the o.d. diameters of the inner tube are 4.76 and 6.35 mm, respectively; whereas those of the outer tube are 10.16 and 12.70 mm, respectively. The axial length of the exchanger is 0.871 m. Saturated water was selected to be the fluid for both the tube flow and the shell flow. Two rotameters were used to measure their inlet volumetric flow rates. Fluid temperatures at inlets and outlets were sensed by four thermocouples in the inlet and the outlet fittings. Since it is impossible to mount two axial fittings at the same location on each side of the exchanger, four tube fittings with two at each end were mounted perpendicular to both tubes to be used as flow entrances and exits. Consequently, fluid flows near both ends of the exchanger are far from being one dimensional and fully developed. In fact, an annular flow with its velocity distribution at either the entrance or the exit being one dimensional is actually unattainable in a laboratory environment.

Results calculated by using the present finite-element analysis (FEM) and by using the classical LMTD method are compared to experimental measurements (EXPR). Both theoretical methods assume that flows in the heat exchanger are fully developed one-dimensional steady laminar flows with constant properties. Thus, Nusselt number of the tube flow is assumed to be 4.364, and that of the shell flow is calculated by interpolating tabulated values reported by Kays[3] for fully developed annular flows. Flow properties are estimated at a mean temperature calculated by averaging the measured inlet and outlet temperatures in both theoretical techniques.

Temperature profiles at the inlets of the fluid flows are assumed to be uniform in the finite element analysis. For both the counterflow and the parallel-flow configurations, the finite element mesh of the computational domain consists of 2400 rectangular elements and 2501 nodes. In the $y$ direction, both the tube-flow domain and the shell-flow domain are divided into 25 elements; whereas the tube-body domain and the shell-body domain are segmented into 5 elements. In the $x$ direction, the entire computational domain is divided into 40 variable-size elements. The element lengths in this direction increase symmetrically from 0.01 at both ends to 0.05 at the center of the exchanger. Since temperatures at the inlet nodes of both the tube flow and the shell flow are given, the total number of nodes with unknown temperature in the computational domain becomes 2449 for both configurations. Therefore, 2449 linear algebraic equations are formed and solved simultaneously in the present analysis.

Table 1 shows the comparison of outlet temperatures as well as values of the heat transfer effectiveness of the parallel-flow (type I) and the counterflow (type II) heat exchangers used for experimental measurements. Results summarized in Table 1 indicate that heat transfer effectiveness estimated from experimental measurements are always higher than those calculated by using both theoretical techniques. However, those obtained by using the FEM are also consistently in better agreement with experimental measurements than those estimated by using the LMTD method. Since the theoretical models assume fully developed one-dimensional flows, but actual flows at the entrances and at the exits are normal to the longitudinal axis of the heat exchanger, it is reasonable to observe higher measured values of heat transfer rate than

**Table 1 Comparison of outlet average temperatures and values of the heat transfer effectiveness of the parallel-flow (type I), as well as the counterflow (type II) heat exchangers used for experimental measurements**

| | | | | | $\bar{T}_{to}$, °F | | | $\bar{T}_{so}$, °F | | | $\varepsilon_t$ | | | $\varepsilon_s$ | | |
|---|---|---|---|---|---|---|---|---|---|---|---|---|---|---|---|---|
| Type | $Re_1$ | $Re_3$ | $\bar{T}_{ti}$, °F | $\bar{T}_{si}$, °F | EXPR | FEM | LMTD | EXPR | FEM | LMTD | EXPR | FEM | LMTD | EXPR | FEM | LMTD |
| I | 1728 | 571 | 102.7 | 65.8 | 91.0 | 93.4 | 94.8 | 72.3 | 72.2 | 70.7 | 0.317 | 0.253 | 0.215 | 0.286 | 0.283 | 0.215 |
| I | 1730 | 406 | 101.8 | 67.9 | 92.1 | 93.7 | 94.8 | 76.5 | 75.9 | 74.3 | 0.286 | 0.238 | 0.207 | 0.281 | 0.262 | 0.207 |
| I | 1313 | 470 | 69.8 | 102.1 | 77.2 | 77.1 | 76.3 | 91.0 | 93.3 | 95.3 | 0.241 | 0.237 | 0.212 | 0.344 | 0.271 | 0.212 |
| I | 1365 | 978 | 69.9 | 112.8 | 83.0 | 80.6 | 79.1 | 104.2 | 105.6 | 107.5 | 0.305 | 0.249 | 0.214 | 0.349 | 0.292 | 0.214 |
| II | 1213 | 620 | 70.1 | 107.0 | 82.8 | 80.7 | 78.7 | 95.0 | 97.9 | 100.6 | 0.344 | 0.286 | 0.233 | 0.436 | 0.332 | 0.233 |
| II | 1567 | 1015 | 69.8 | 113.7 | 88.0 | 81.1 | 78.5 | 102.0 | 105.6 | 108.4 | 0.415 | 0.258 | 0.198 | 0.436 | 0.304 | 0.198 |
| II | 1956 | 595 | 105.8 | 66.2 | 95.0 | 95.4 | 97.8 | 75.0 | 74.0 | 71.5 | 0.273 | 0.262 | 0.202 | 0.338 | 0.300 | 0.202 |
| II | 1688 | 398 | 103.0 | 67.9 | 92.5 | 93.4 | 95.4 | 78.2 | 77.5 | 74.8 | 0.299 | 0.272 | 0.217 | 0.326 | 0.302 | 0.217 |

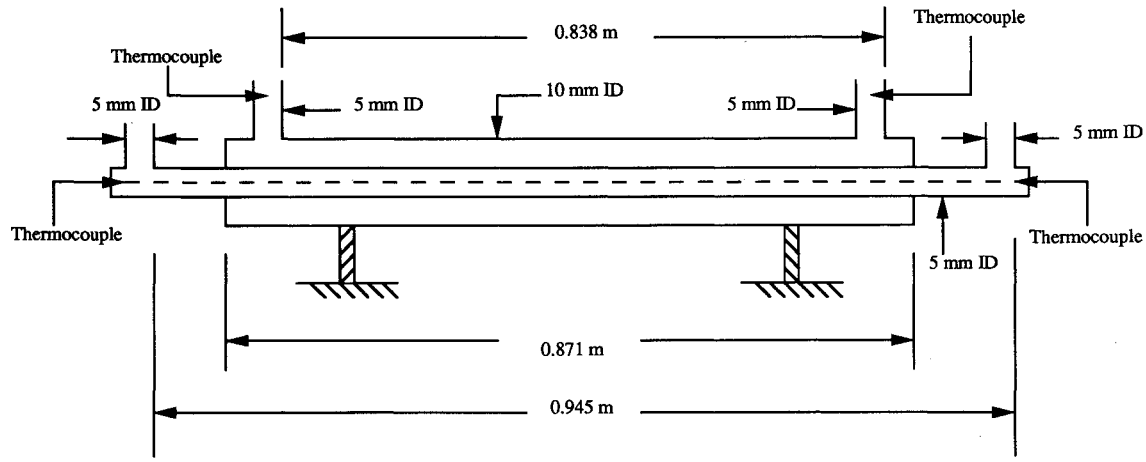


**Fig. 1 Schematic of the experimental apparatus.**

**Table 2 Influence of the conduction and the viscous dissipation upon the finite element results for the parallel-flow (type I) and the counterflow (type II) heat exchangers**

| Type | $Re_1$ | $Re_3$ | $\bar{T}_{ti}$, °F | $\bar{T}_{si}$, °F | Terms neglected | $\bar{T}_{to}$, °F | $\bar{T}_{so}$, °F | $\varepsilon_t$ | $\varepsilon_s$ |
|---|---|---|---|---|---|---|---|---|---|
| I | 1728 | 571 | 102.7 | 65.8 | None | 93.4 | 72.2 | 0.253 | 0.283 |
| | | | | | Solid conduction | 93.2 | 71.8 | 0.256 | 0.264 |
| | | | | | Fluid conduction | 93.4 | 72.2 | 0.253 | 0.283 |
| | | | | | Dissipation | 93.4 | 72.3 | 0.251 | 0.285 |
| II | 1213 | 620 | 70.1 | 107.0 | None | 80.7 | 97.9 | 0.286 | 0.332 |
| | | | | | Solid conduction | 80.8 | 98.5 | 0.290 | 0.310 |
| | | | | | Fluid conduction | 80.7 | 97.9 | 0.287 | 0.332 |
| | | | | | Dissipation | 80.7 | 97.7 | 0.287 | 0.331 |

those calculated by using an idealistic model. Therefore, moderate disagreements observed between the finite element predictions and the experimental measurements are considered reasonable. The finite element technique, in general, can predict more realistic results than the LMTD method does.

Table 2 shows the effects of the viscous dissipation as well as the axial conduction upon the calculated values of the effectiveness and outlet temperatures using the present finite-element method. It is obvious that the effect of the axial conduction of the fluid media is very insignificant; however, neglecting the solid-body conduction terms can yield significantly different values of the heat transfer effectiveness and outlet temperatures. Although viscous-dissipation terms can be considered, their influences are actually almost negligible.

## Conclusions

Although there are moderate disagreements between the experimental measurements and the finite element results, they are primarily due to experimental uncertainties, as well as due to the change of flow directions at the entrances and at the exits in the experimental setup. The technique, in general, can predict more realistic results than the classical LMTD method does. In addition, the temperature distribution in the heat exchanger can also be easily determined by using the finite element analysis. However, the method is still far from becoming a practical design tool because it can only be used to solve simple and idealistic cases up to this date.

Although the viscous-dissipation and the axial-conduction terms of the fluid flows in the heat exchanger are included in the present analysis, numerical results obtained have confirmed the validity of the generally accepted notion that their effects upon the final results are negligibly small.

## References

[1]Mikhailov, M. D., and Ozisik, M. N., "Finite Element Analysis of Heat Exchangers," *Heat Exchangers, Thermal-Hydraulic Fundamentals and Design*, edited by S. Kakac, A. E. Bergles, and F. Mayinger, McGraw-Hill, New York, 1981, pp. 461–479.

[2]White, F. M., *Fluid Mechanics*, McGraw-Hill, New York, 1986, Chap. 6.

[3]Kays, W. M., *Convective Heat and Mass Transfer*, McGraw-Hill, New York, 1966, Chap. 8.